# Dephasing of electrons in mesoscopic metal wires

F. Pierre,[1,2,3,*] A. B. Gougam,[1,†] A. Anthore,[2] H. Pothier,[2] D. Esteve,[2] and Norman O. Birge[1]
[1]*Department of Physics and Astronomy, Michigan State University, East Lansing, Michigan 48824-2320, USA*
[2]*Service de Physique de l'Etat Condensé, Direction des Sciences de la Matière, CEA-Saclay, 91191 Gif-sur-Yvette, France*
[3]*Department of Applied Physics, Yale University, New Haven, Connecticut 06520, USA*
(Received 11 February 2003; published 26 August 2003)

We have extracted the phase coherence time $\tau_\phi$ of electronic quasiparticles from the low field magnetoresistance of weakly disordered wires made of silver, copper, and gold. In samples fabricated using our purest silver and gold sources, $\tau_\phi$ increases as $T^{-2/3}$ when the temperature $T$ is reduced, as predicted by the theory of electron–electron interactions in diffusive wires. In contrast, samples made of a silver source material of lesser purity or of copper exhibit an apparent saturation of $\tau_\phi$ starting between 0.1 and 1 K down to our base temperature of 40 mK. By implanting manganese impurities in silver wires, we show that even a minute concentration of magnetic impurities having a small Kondo temperature can lead to a quasisaturation of $\tau_\phi$ over a broad temperature range, while the resistance increase expected from the Kondo effect remains hidden by a large background. We also measured the conductance of Aharonov–Bohm rings fabricated using a very pure copper source and found that the amplitude of the $h/e$ conductance oscillations increases strongly with magnetic field. This set of experiments suggests that the frequently observed ''saturation'' of $\tau_\phi$ in weakly disordered metallic thin films can be attributed to spin–flip scattering from extremely dilute magnetic impurities, at a level undetectable by other means.

DOI: 10.1103/PhysRevB.68.085413 PACS number(s): 73.23.−b, 73.50.−h, 71.10.Ay, 72.70.+m

## I. MOTIVATIONS

The time $\tau_\phi$ during which the quantum coherence of an electron is maintained is of fundamental importance in mesoscopic physics. The observability of many phenomena specific to this field relies on a long enough phase coherence time.[1] Amongst these are the weak localization correction to the conductance (WL), the universal conductance fluctuations (UCF), the Aharonov-Bohm (AB) effect, persistent currents in rings, the proximity effect near the interface between a superconductor and a normal metal, and others. Hence it is crucial to find out what mechanisms limit the quantum coherence of electrons.

In metallic thin films, at low temperature, electrons experience mostly elastic collisions from sample boundaries, defects of the ion lattice and static impurities in the metal. These collisions do not destroy the quantum coherence of electrons. Instead they can be pictured as resulting from a static potential on which the diffusivelike electronic quantum states are built.

What limits the quantum coherence of electrons are inelastic collisions. These are collisions with other electrons through the screened Coulomb interaction, with phonons, and also with extrinsic sources such as magnetic impurities or two level systems in the metal. Whereas above about 1 K electron–phonon interactions are known to be the dominant source of decoherence,[2] electron–electron interactions are expected to be the leading inelastic process at lower temperatures in samples without extrinsic sources of decoherence.[3]

The theory of electron–electron interactions in the diffusive regime was worked out in the early 1980s (for a review, see Ref. 4). It predicts a power law divergence of $\tau_\phi$ when the temperature $T$ goes to zero. Effects of quantum interference are therefore expected to grow significantly upon cooling down the electrons. In mesoscopic wires, the predicted power law $\tau_\phi \propto T^{-2/3}$ was first observed in 1986 by Wind *et al.*[5] between 2 K and 5 K in aluminum and silver wires and then by Echternach *et al.*[6] down to 100 mK in a gold wire. However, in 1997, Mohanty, Jariwala, and Webb[7] published a series of measurements of $\tau_\phi$ on gold wires with a broad range of diffusion coefficients. They observed that the phase coherence time tends to saturate at low temperature, typically below 0.5 K, in apparent contradiction with theoretical predictions. That same year, measurements of the energy exchange rate between electrons in copper wires[8] were found to be at odds, both qualitatively and quantitatively, with the prediction for electron–electron interactions. Both experiments suggested that electrons in mesoscopic metallic wires interact with each other differently and more strongly than predicted by theory.

To shed some light on this issue we present here several sets of experiments probing the phase coherence time at low temperature in mesoscopic metal wires.[9] We summarize our most important conclusions here. First, we measured $\tau_\phi(T)$ down to 40 mK in several wires made of copper, silver, and gold and fabricated from source materials of various purities. We found in the four very pure silver wires and in the very pure gold wire that $\tau_\phi(T)$ does not saturate in the investigated temperature range, but continues to increase as the temperature is lowered in agreement with the theoretical prediction. Since these samples have comparable resistances and geometries as some measured in Ref. 7, this observation casts doubt on the assertion[7] that saturation of $\tau_\phi$ is a universal feature of weakly-disordered metals. Second, we tested the impact of very dilute magnetic impurities with a small Kondo temperature on the temperature dependence of $\tau_\phi$. We found that even at concentrations lower than one part per million (1 ppm), such impurities can cause $\tau_\phi(T)$ to display a plateau over a large temperature range. This could explain why saturation of $\tau_\phi$ at low temperature is frequently

 

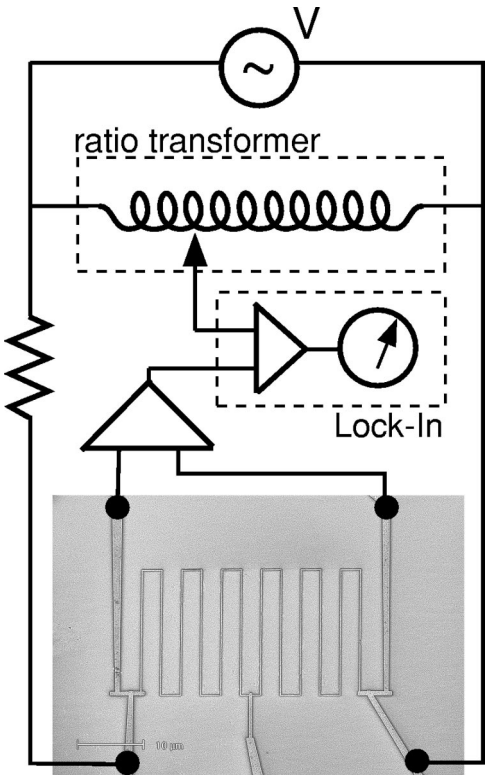


FIG. 1. Photograph of a silver sample taken with a scanning electron microscope, and schematic of measurement circuit. The wire resistance is obtained by a four-lead measurement in a bridge configuration: the current is injected by two arms through the bias resistor and the voltage is measured across two other arms in order to probe only the wire resistance; a ratio transformer is used to enhance sensitivity to small variations of the sample resistance.

observed. Finally, we probed the magnetic field dependence of the phase coherence time by measuring the magnetoresistance of copper Aharonov-Bohm rings showing a temperature-independent $\tau_\phi$ at low temperature. The amplitude of the Aharonov-Bohm conductance oscillations increased strongly on a field scale proportional to the temperature, indicating that the phase coherence time at zero field was limited by spin-flip scattering from magnetic impurities.

## II. EXPERIMENTAL TECHNIQUES

### A. Sample fabrication

Figure 1 displays the photograph of a typical sample together with a schematic of the measurement setup.

All samples were fabricated using standard e-beam lithography techniques. A bilayer resist, consisting of a copolymer P(MMA/MAA) bottom layer and a PMMA top layer, was first spun onto an oxidized Si substrate wafer. This bilayer was then patterned by e-beam lithography to tailor a mask. The metal—gold, copper, or silver—was deposited directly through this mask in evaporators used only for nonmagnetic metals.[10]

Samples made at Saclay used a Si substrate thermally oxidized over 500 nm, and metal evaporation was performed in an electron gun evaporator. The silver source material was placed inside a carbon liner, whereas copper and gold were put directly in the buckets of the e-gun system. Metal evaporation took place at a base pressure of about $10^{-6}$ mbar with an evaporation rate of 0.2, 0.5, and 1 nm/s for silver, gold, and copper, respectively (see Ref. 11).

Samples made at Michigan State University (MSU) were evaporated on a Si substrate with only the native oxide in a thermal evaporator used only for silver, aluminum, gold, copper and titanium. The source material and boat were replaced before each evaporation and manipulated using plastic tweezers. The pressure during evaporation was about $10^{-6}$ mbar and the evaporation rate ranged between 0.2 and 0.5 nm/s.[12]

We measured the low field magnetoresistance of copper, gold, and silver wires fabricated using source materials of purity 99.999% (5N) and 99.9999% (6N). Electrical and geometrical characteristics of the samples are summarized in Table I.

TABLE I. Geometrical and electrical characteristics of the measured samples (Ref. 14). The diffusion coefficient $D$ is obtained using Einstein's relation $1/\rho = \nu_F e^2 D$ with the density of states in copper, silver and gold respectively $\nu_F = 1.56\times10^{47}$, $1.03\times10^{47}$, and $1.14\times10^{47}$ $J^{-1}\,m^{-3}$, and the resistivity $\rho$ extracted from the resistance $R$, thickness $t$, length $L$, and width $w$ of the long wire. Length and width were measured with a scanning electron microscope (SEM). The thickness of most samples was measured with an atomic force microscope (AFM); for others the value given by a calibrated thickness monitor in the evaporator was used. A rectangular cross section is assumed.

| Sample | Made at | $L$ ($\mu$m) | $t$ (nm) | $w$ (nm) | $R$ (k$\Omega$) | $D$ (cm$^2$/s) |
|---|---|---|---|---|---|---|
| Ag(6N)a | Saclay | 135 | 45 | 65 | 1.44 | 115 |
| Ag(6N)b | Saclay | 270 | 45 | 100 | 3.30 | 70 |
| Ag(6N)c | Saclay | 400 | 55 | 105 | 1.44 | 185 |
| Ag(6N)d | MSU | 285 | 35 | 90 | 1.99 | 165 |
| Ag(5N)a | Saclay | 135 | 65 | 108 | 0.68 | 105 |
| Ag(5N)b | Saclay | 270 | 65 | 90 | 1.31 | 135 |
| Ag(5N)$c_{Mn0.3}$ | Saclay | 135 | 65 | 110 | 0.47 | 150 |
| Ag(5N)$d_{Mn1}$ | Saclay | 270 | 65 | 95 | 1.22 | 135 |
| Au(6N) | MSU | 175 | 45 | 90 | 1.08 | 135 |
| Cu(6N)a | MSU | 285 | 45 | 155 | 0.70 | 145 |
| Cu(6N)b | MSU | 285 | 20 | 70 | 7.98 | 60 |
| Cu(6N)c | MSU | 285 | 35 | 75 | 4.37 | 65 |
| Cu(6N)d | MSU | 285 | 20 | 80 | 8.50 | 50 |
| Cu(5N)a | Saclay | 270 | 45 | 110 | 1.68 | 70 |
| Cu(5N)b | Saclay | 270 | 45 | 100 | 0.95 | 160 |

### B. Experimental setup

The samples were immersed in the mixing chamber of a top loading dilution refrigerator. Electrical lines to the sample were filtered by commercial ''pi'' filters at the top of the cryostat and by discrete RC filters in the mixing chamber. Resistance measurements were performed using a standard ac four-terminal technique with a room temperature preamplifier of input voltage noise 1.5 nV/$\sqrt{\text{Hz}}$ and a lock-in am-

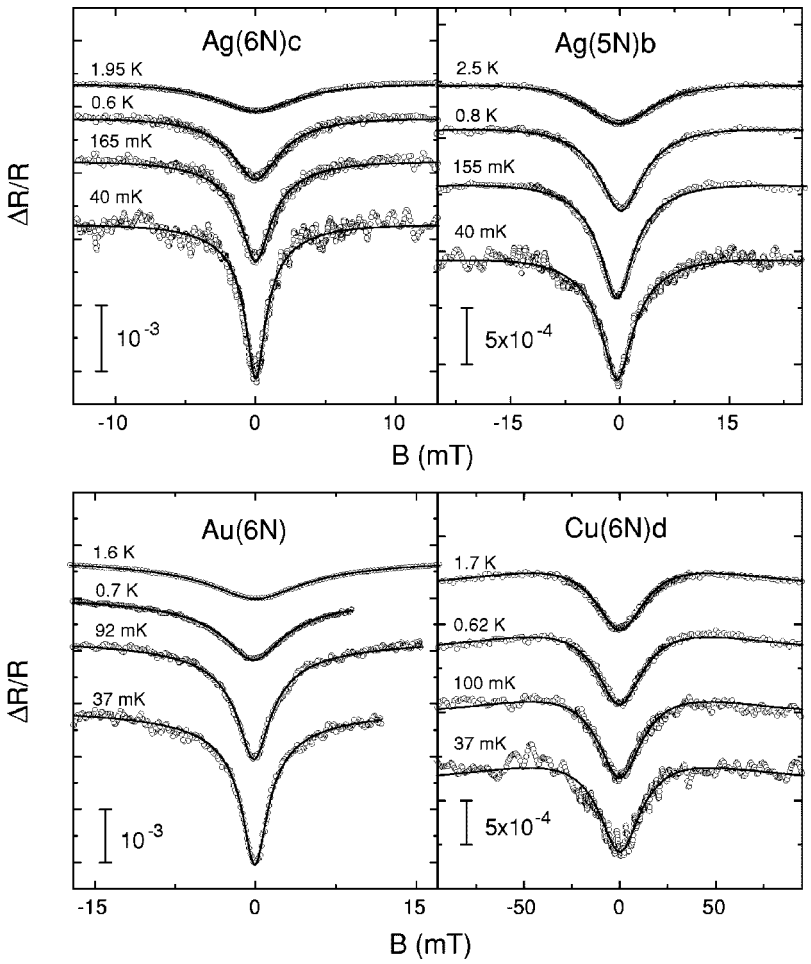


FIG. 2. Magnetoresistance data (symbols) and fits to Eq. (1) (solid lines). Top panels are measurements of two silver samples made of source materials of nominal purity 6N (99.9999%, top left panel) and 5N (99.999%, top right panel). Bottom panels display data measured on gold (bottom left panel) and copper (bottom right panel) samples made of 6N nominal purity source materials. The curves are offset vertically for clarity.

plifier operated at frequencies between 100 and 300 Hz (see Fig. 1). To avoid significant heating of electrons we used ac voltages $V_{ac}$ across the samples such that $eV_{ac} \lesssim k_B T$. This is particularly important at temperatures below 100 mK for which the length scale for electron–phonon interactions, responsible for cooling down the electronic fluid, can be as large as several millimeters (see Appendix A). A bridge circuit with a ratio transformer on one arm was used to enhance the measurement sensitivity to small changes in sample resistance. A magnetic field was applied perpendicular to the plane of the sample using a superconducting coil.

### III. LOW FIELD MAGNETORESISTANCE MEASUREMENTS

The most accurate way to extract $\tau_\phi$ at low magnetic field in metallic thin films is to measure the magnetoresistance and to fit it using weak localization theory.[13] Both the amplitude and width of the weak localization peak (dip when spin–orbit coupling is strong) in the resistance are sensitive to the phase coherence length.

Figure 2 displays the low field magnetoresistance of samples Ag(6N)c, Ag(5N)b, Au(6N), and Cu(6N)d at several temperatures. The positive magnetoresistance indicates that spin–orbit scattering is stronger than inelastic scattering ($\tau_{so} < \tau_\phi$). Raw magnetoresistance measurements already reveal a qualitative difference between these samples: the dip in the magnetoresistance of samples Ag(6N)c and Au(6N) becomes deeper and narrower upon cooling down to base temperature whereas it stops changing at low temperature in samples Ag(5N)b and Cu(6N)d.

The magnetoresistance $\Delta R \equiv R(B) - R(\infty)$ is fit with the quasi-1D expression for the weak localization correction,

$$\frac{\Delta R}{R} = \frac{2R}{R_K L}\left\{\frac{3}{2}\left[\frac{1}{L_\phi^2} + \frac{4}{3L_{so}^2} + \frac{1}{3}\left(\frac{w}{L_H^2}\right)^2\right]^{-1/2} - \frac{1}{2}\left[\frac{1}{L_\phi^2} + \frac{1}{3}\left(\frac{w}{L_H^2}\right)^2\right]^{-1/2}\right\}, \quad (1)$$

where $R$ is the resistance of a wire of length $L$ and width $w$, $R_K = h/e^2$ is the resistance quantum, $L_\phi = \sqrt{D\tau_\phi}$ is the phase coherence length, $D$ is the diffusion coefficient of electrons, $L_H = \sqrt{\hbar/eB}$ is the magnetic length, $B$ is the magnetic field applied perpendicularly to the sample plane, and $L_{so} = \sqrt{D\tau_{so}}$ is the spin–orbit length that characterizes the intensity of spin–orbit coupling. Expression (1) holds for metallic wires in the diffusive regime, far from the metal–insulator transition, and in the quasi-1D regime, $l_e \ll w, t \ll L_H, L_\phi, L_{so} \ll L$, with $t$ the sample thickness and $l_e$ the elastic mean free path of electrons (see Refs. 15,16 and Appendix B).

TABLE II. Fit parameters of the magnetoresistance data to weak localization theory: maximum phase coherence time $\tau_\phi^{\max}$, obtained at the lowest temperature of ~40 mK; spin–orbit length $L_{so}$ and effective width $w_{WL}$. We also recall the width $w$ obtained from SEM pictures. The upwards arrow ↗ indicates that $\tau_\phi$ keeps increasing down to 40 mK. In the other samples, $\tau_\phi$ is nearly constant at low temperature.

| Sample | $\tau_\phi^{\max}$ (ns) | $L_{so}$ ($\mu$m) | $w_{WL}$ ($w$) (nm) |
|---|---|---|---|
| Ag(6N)a | 9↗ | 0.65 | 57 (65) |
| Ag(6N)b | 12↗ | 0.35 | 85 (100) |
| Ag(6N)c | 22↗ | 1.0 | 90 (105) |
| Ag(6N)d | 12↗ | 0.82 | 75 (90) |
| Ag(5N)a | 2.9 | 0.65 | 108 (108) |
| Ag(5N)b | 3.5 | 0.75 | 82 (90) |
| Au(6N) | 11↗ | 0.085 | 85 (90) |
| Cu(6N)a | 0.45 | 0.67 | 155 (155) |
| Cu(6N)b | 0.95 | 0.4 | 70 (70) |
| Cu(6N)c | 0.2 | 0.35 | 75 (75) |
| Cu(6N)d | 0.35 | 0.33 | 80 (80) |
| Cu(5N)a | 1.8 | 0.52 | 110 (110) |
| Cu(5N)b | 0.9 | 0.67 | 100 (100) |

In the fit procedure, we use the measured sample resistance and length given in Table I. Our experimental setup being designed to measure resistance changes with an higher accuracy than absolute values, $\Delta R$ is known only up to a small additive constant that we adjusted to fit each magnetoresistance curve. The width was fixed at a value $w_{WL}$ giving the best overall fits for the complete set of data at various temperatures. The difference between the width $w$ measured from scanning electron microscope images and the best fit value $w_{WL}$ (see Table II) was found to be always less than 15%.[17] The spin–orbit length $L_{so}$ was obtained from fits of the magnetoresistance measured at the highest temperature. These parameters being determined, $L_\phi$ remains as the only fit parameter for each magnetoresistance curve. Examples of fits are displayed as solid lines in Fig. 2.

In order to get $\tau_\phi$ from $L_\phi$, the diffusion coefficient $D$ was determined using the measured geometrical and electrical sample characteristics given in Table I. Figure 3 shows $\tau_\phi$ as a function of temperature for samples Ag(6N)c, Ag(5N)b, Au(6N), and Cu(6N)b. This confirms quantitatively the differences between samples already mentioned from the raw magnetoresistance data. On the one hand, the samples Ag(6N)c and Au(6N), fabricated using our purest (6N) silver and gold sources, present a large phase coherence time that keeps increasing at low temperature. On the other hand, the copper sample Cu(6N)b and the sample Ag(5N)b, fabricated using a silver source of smaller nominal purity (5N), present a much smaller phase coherence time and exhibit a plateau in $\tau_\phi(T)$, in contradiction with the theoretical prediction for electron–electron interactions. This trend, illustrated in Fig. 3, has been confirmed by the measurements of several samples, as summarized in Table II.

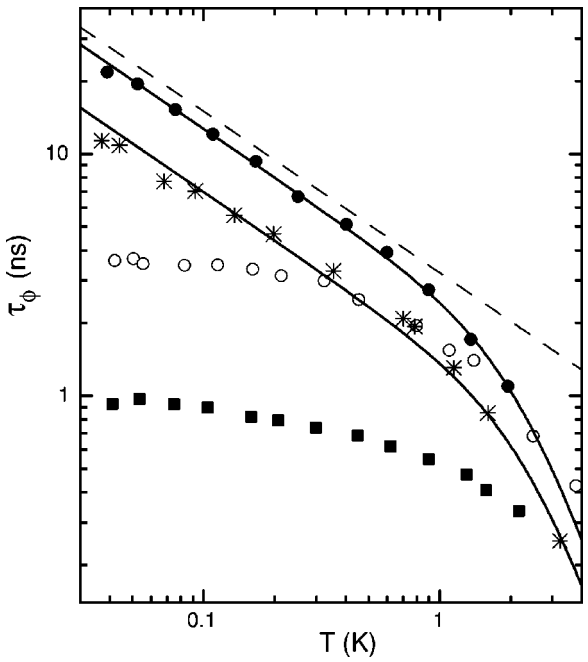


FIG. 3. Phase coherence time $\tau_\phi$ versus temperature in wires made of copper Cu(6N)b (■), gold Au(6N) (*), and silver Ag(6N)c (●) and Ag(5N)b (○). The phase coherence time increases continuously with decreasing temperature in wires fabricated using our purest (6N) silver and gold sources as illustrated respectively with samples Ag(6N)c and Au(6N). Continuous lines are fits of the measured phase coherence time including inelastic collisions with electrons and phonons [Eq. (4)]. The dashed line is the prediction of electron–electron interactions only [Eq. (3)] for sample Ag(6N)c. In contrast, the phase coherence time increases much more slowly in samples made of copper (independently of the source material purity) and in samples made of silver using our source of lower (5N) nominal purity.

## IV. COMPARISON WITH THEORETICAL PREDICTIONS AND DISCUSSION

### A. Purest silver and gold samples

Theory predicts that, in samples without extrinsic sources of decoherence, $\tau_\phi(T)$ is limited by the contributions of electron–electron $\tau_{ee}$ and electron–phonon $\tau_{ph}$ interactions. In principle, decoherence by electron–electron scattering is not purely an exponential process, hence the decoherence rates from electron–electron and electron–phonon scattering do not simply add. In practice (see Appendix B), the exact formula for the magnetoresistance is indistinguishable from Eq. (1) with a total decoherence rate,

$$\frac{1}{\tau_\phi(T)} = \frac{1}{\tau_{ee}(T)} + \frac{1}{\tau_{ph}(T)}. \tag{2}$$

For our wires, whose width and thickness are smaller than $L_\phi$, the quasi-1D prediction for electron–electron interactions applies[15]

$$\tau_{ee} = \hbar \left[ \frac{(4/\pi)(R_K/R)\nu_F SL}{(k_B T)^2} \right]^{1/3} \equiv \frac{1}{A_{thy} T^{2/3}}, \tag{3}$$

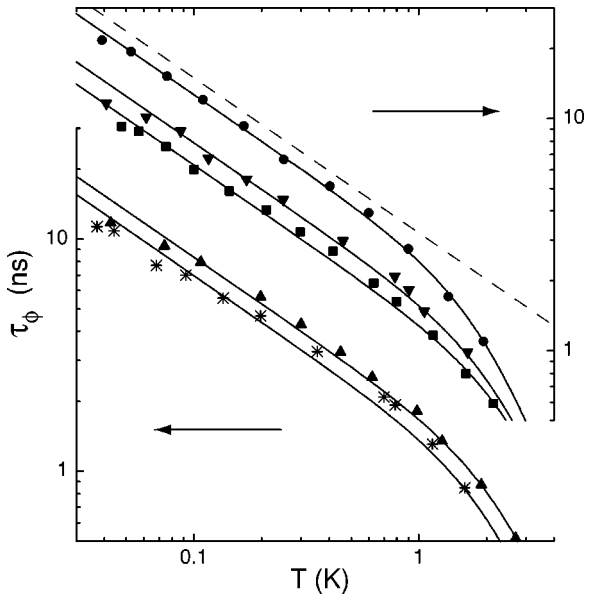


FIG. 4. Phase coherence time vs temperature in samples Ag(6N)a (■), Ag(6N)b (▼), Ag(6N)c (●), Ag(6N)d (▲), and Au(6N) (*), all made of 6N sources. Continuous lines are fits of the data to Eq. (4). For clarity, the graph has been split in two part, shifted vertically one with respect to the other. The quantitative prediction of Eq. (3) for electron–electron interactions in sample Ag(6N)c is shown as a dashed line.

where $\nu_F$ is the density of states per unit volume at the Fermi energy, and $S$ is the cross section of the wire.

In order to test the theoretical predictions, the measured $\tau_\phi(T)$ curves were fit with the functional form,

$$\tau_\phi^{-1} = AT^{2/3} + BT^3, \tag{4}$$

where the second term describes electron–phonon scattering, dominant at higher temperatures.[2] Fits are shown as continuous lines in Fig. 4 (the fit parameters minimize the distance between the data points and the fit curve in a log–log plot). Equation (4) describes accurately the temperature dependence of $\tau_\phi(T)$ for samples Ag(6N)a, b, c and, with a slightly reduced fidelity, for samples Ag(6N)d and sample Au(6N). In all these samples, fabricated using 6N source materials of silver and gold, $\tau_\phi(T)$ follows very closely, below about 1 K, the $1/T^{2/3}$ dependence expected when the electron–electron interaction is the dominant inelastic process. Nevertheless, if the exponent of $T$ is left as a fit parameter, better fits are obtained with smaller exponents ranging from 0.59 for samples Ag(6N)d and Au(6N) up to 0.64 for sample Ag(6N)c. This issue will be discussed in Sec. V B. The dashed line in Fig. 3 and Fig. 4 is the quantitative prediction of Eq. (3) for electron–electron interactions in sample Ag(6N)c. The dephasing times are close, though always slightly smaller, to the theoretical prediction of Eq. (3). Table III lists the best fit parameters $A$, $B$, together with the prediction $A_{\rm thy}$ of Eq. (3).

TABLE III. Theoretical predictions of Eq. (3) and fit parameters for $\tau_\phi(T)$ in the purest silver and gold samples using the functional form given by Eq. (4).

| Sample | $A_{\rm thy}$ ($\rm ns^{-1}\,K^{-2/3}$) | $A$ ($\rm ns^{-1}\,K^{-2/3}$) | $B$ ($\rm ns^{-1}\,K^{-3}$) |
|---|---|---|---|
| Ag(6N)a | 0.55 | 0.73 | 0.045 |
| Ag(6N)b | 0.51 | 0.59 | 0.05 |
| Ag(6N)c | 0.31 | 0.37 | 0.047 |
| Ag(6N)d | 0.47 | 0.56 | 0.044 |
| Au(6N) | 0.40 | 0.67 | 0.069 |

This data set casts doubt on the claim by Mohanty, Jariwala, and Webb[7] (MJW) that saturation of $\tau_\phi$ is a universal phenomenon in mesoscopic wires. One can always argue that the saturation temperature for our silver samples is below 40 mK, hence unobservable in our experiments. However, the resistivity and dimensions of sample Ag(6N)a are similar to those of sample Au-3 in the MJW paper,[7] which exhibits saturation of $\tau_\phi$ starting at about 100 mK, and has a maximum value of $\tau_\phi^{\rm max}=2$ ns. In contrast, $\tau_\phi$ reaches 9 ns in Ag(6N)a.

### B. Silver 5N and copper samples

In silver samples made from a 5N purity source, the phase coherence time is systematically shorter than predicted by Eq. (3) and displays an unexpectedly flat temperature dependence below 400 mK. The same is true for all the copper samples we measured, independently of source purity.[18] These trends are illustrated for samples Ag(5N)b and Cu(6N)b in Fig. 3.

What can be responsible for this anomalous behavior? There have been several theoretical suggestions regarding sources of extra dephasing. Some of these, such as the presence of a parasitic high frequency electromagnetic radiation,[19] can be ruled out purely on experimental grounds. Indeed some samples do show a saturation of $\tau_\phi$, while others of similar resistance and geometry, measured in the same cryostat, do not. This indicates that, in our experiments at least, the observed excess dephasing is not an artifact of the measurement. The main suggestions to explain the anomalous behavior of $\tau_\phi$ are dephasing by very dilute magnetic impurities,[11,20] dephasing by two-level systems associated with lattice defects,[21,22] and dephasing by electron–electron interactions through high energy electromagnetic modes.[23]

The correlation between source material purity and excess dephasing amongst silver samples fabricated using the exact same process but with either our 5N or 6N source material suggests that impurities are responsible for the anomalous temperature dependence of $\tau_\phi$. The fact that, among all the 6N silver samples, $\tau_\phi(T)$ deviates the most from the prediction of electron–electron interactions in Ag(6N)d, fabricated in MSU (see Fig. 4) would mean that the 6N silver source material used at MSU contains more ''dangerous'' impurities than the one at Saclay.

The phase coherence time in the copper samples is always almost independent of temperature below about 200 mK down to our base temperature of 40 mK (see Refs. 11,24,25). However, as opposed to silver samples, this unexpected be-

TABLE IV. Kondo temperature $T_K$ (K) of common, low $T_K$, magnetic impurities in Ag, Au, and Cu (taken from Ref. 27).

| Host \ Impurity | Cr | Fe | Mn |
|---|---|---|---|
| Ag | ~0.02 | ~3 | 0.04 |
| Au | ~0.01 | 0.3 | <0.01 |
| Cu | 1.0 | 25 | 0.01 |

havior is not correlated with the source material purity (5N or 6N). A likely explanation is provided by early measurements showing that the surface oxide of copper can cause dephasing.[26]

## V. INFLUENCE ON $\tau_\phi$ OF VERY DILUTE MAGNETIC IMPURITIES

Dephasing of conduction electrons by paramagnetic impurities has been known since 1980,[20] hence it may come as a surprise that this issue is still under debate today. In their Letter on the "saturation" of $\tau_\phi$ at low temperature,[7] Mohanty, Jariwala, and Webb studied the effect of intentionally doping their gold wires with iron impurities. They found that $\tau_\phi$ in those samples did not truly saturate, but rather reached a plateau around 1 K and increased again below about 0.3 K. In addition, the presence of the iron impurities could be detected by a logarithmic contribution to the temperature dependence of the resistance $R(T)$, known as the Kondo effect. They concluded from those data that magnetic impurities were not the cause of the saturation of $\tau_\phi$ they observed in their nominally pure gold samples. However, it is well known that the spin-flip scattering rate peaks near the Kondo temperature $T_K$, then decreases at lower temperature. While MJW showed convincingly that "saturation" of $\tau_\phi$ in gold could not be caused by iron impurities with $T_K \approx 0.3$ K, their data do not exclude an effect of impurities with a lower Kondo temperature, such as manganese or chromium (see Table IV).

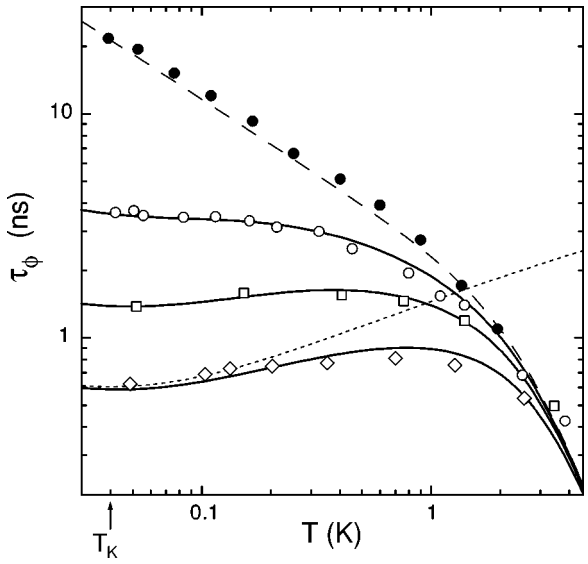


FIG. 5. Phase coherence time as function of temperature in several silver wires. Sample Ag(6N)c (●) is made of the purest silver source. Samples Ag(5N)b (○), Ag(5N)$c_{Mn0.3}$ (□), and Ag(5N)$d_{Mn1}$ (◇) were evaporated simultaneously using our 5N silver source. Afterward, 0.3 ppm and 1 ppm of manganese was added by ion implantation respectively in samples Ag(5N)$c_{Mn0.3}$ and Ag(5N)$d_{Mn1}$. The presence of very dilute manganese atoms, a magnetic impurity of Kondo temperature $T_K = 40$ mK, reduces $\tau_\phi$ leading to an apparent "saturation" at low temperature. Continuous lines are fits of $\tau_\phi(T)$ taking into account the contributions of electron–electron and electron–phonon interactions (dashed line) and spin–flip collisions using the concentration $c_{mag}$ of magnetic impurity as a fit parameter (dotted line is $\tau_{sf}$ for $c_{mag} = 1$ ppm). Best fits are obtained using $c_{mag} = 0.13$, 0.39, and 0.96 ppm, respectively, for samples Ag(5N)b, Ag(5N)$c_{Mn0.3}$, and Ag(5N)$d_{Mn1}$, in close agreement with the concentrations implanted and consistent with the source material purity used.

### A. Can dilute magnetic impurities account for a plateau in $\tau_\phi(T)$?

To answer this question experimentally, we fabricated simultaneously three silver samples Ag(5N)b, Ag(5N)$c_{Mn0.3}$, and Ag(5N)$d_{Mn1}$, and very dilute manganese atoms were introduced by ion implantation[28] in two of them. Manganese atoms form Kondo impurities in silver with a Kondo temperature $T_K \simeq 40$ mK.

The phase coherence times extracted from WL corrections are shown as symbols in Fig. 5. Samples Ag(6N)c, evaporated separately, is shown as a reference. At the time of this experiment only the 5N purity silver source was available. Sample Ag(5N)b, in which no manganese atoms were implanted, already shows very little temperature dependence of $\tau_\phi \sim 3.5$ ns below 0.3 K. Nevertheless, introducing more manganese reduces further the phase coherence time as illustrated with samples Ag(5N)$c_{Mn0.3}$ and Ag(5N)$d_{Mn1}$ in which, respectively, 0.3 and 1 ppm of manganese were implanted. For instance, by adding 1 ppm of manganese, $\tau_\phi$ was reduced by a factor of 6 while leaving $\tau_\phi$ still nearly independent of temperature.

The effect of manganese on $\tau_\phi$ is now compared with the existing theory of spin–flip scattering in the Kondo regime.

### B. Comparison with the theory of spin–flip scattering

In the presence of spin–flip scattering the phase coherence time reads

$$\frac{1}{\tau_\phi} = \frac{1}{\tau_{ee}} + \frac{1}{\tau_{ph}} + \frac{1}{\tau_{sf}}, \tag{5}$$

where $1/\tau_{sf}$ is the spin–flip rate of electrons. This expression is valid when the spin–flip scattering time of the conduction electrons is longer than the spin relaxation time ($\tau_K$ for Korringa time) of the magnetic impurities themselves, i.e., $\tau_{sf} > \tau_K$.[29] This holds if

$$T \gtrsim \frac{c_{mag}}{\nu_F k_B}, \tag{6}$$

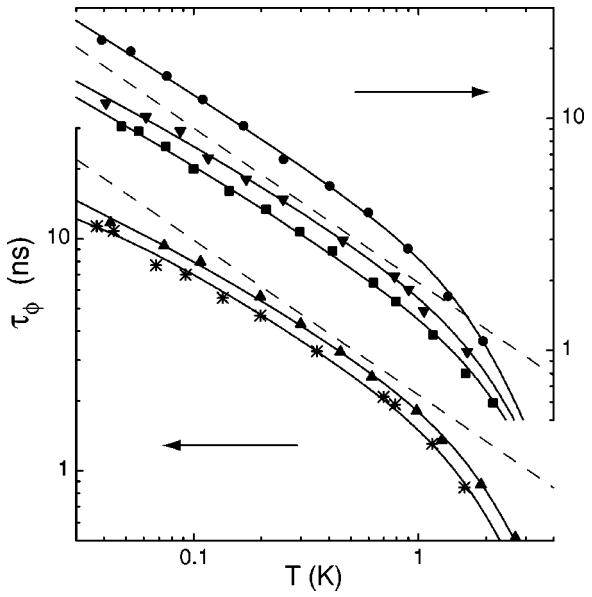


FIG. 6. Phase coherence time vs temperature measured on samples Ag(6N)a (■), Ag(6N)b (▼), Ag(6N)c (●), Ag(6N)d (▲), and Au(6N) (*). For clarity the graph has been split in two parts shifted vertically, as was done in Fig. 4. In contrast to Fig. 4, continuous lines are fits of the data to Eqs. (5) and (8), with the concentration of magnetic impurities as an additional fit parameter (see Table V). The quantitative prediction of Eq. (3) for electron–electron interactions in samples Ag(6N)b (top part) and Ag(6N)d (bottom part) are shown as dashed lines.

where $c_{\rm mag}$ is the concentration per unit volume of magnetic impurities. In silver, gold, and copper this criterion reads

$$T \gtrsim 40 \ \ {\rm mK} \times c_{\rm mag}({\rm ppm}), \tag{7}$$

in which $c_{\rm mag}$(ppm) is now written in parts per million atoms (ppm). In the opposite limit ($\tau_{\rm sf} < \tau_K$), the impact of spin flip scattering on $\tau_\phi$ depends on the physical effect probed. For weak localization corrections with strong spin–orbit coupling, spin–flip scattering enters then as $2/\tau_{\rm sf}$ in Eq. (5).[20,29]

As long as $T \gtrsim T_K$, $\tau_{\rm sf}$ is well described by the Nagaoka-Suhl formula[30,31]

$$\frac{1}{\tau_{\rm sf}} = \frac{c_{\rm mag}}{\pi \hbar \nu_F} \frac{\pi^2 S(S+1)}{\pi^2 S(S+1) + \ln^2(T/T_K)}, \tag{8}$$

with $S$ and $T_K$, respectively, the spin and Kondo temperature of the magnetic impurities.

Upon cooling down, $\tau_{\rm sf}$ decreases when $T$ approaches $T_K$ (dotted line in Fig. 5), whereas the electron–electron scattering time $\tau_{ee}$ increases. The combination of both contributions can result in a nearly constant phase coherence time above $T_K$, as shown by the solid lines in Fig. 5.

A quick way to estimate the concentration of magnetic impurities corresponding to a plateau in the phase coherence time is to compare $\tau_\phi^{\rm plateau}$ at the plateau to the prediction of Nagaoka-Suhl at $T = T_K$. In samples made of copper, gold and silver this gives

$$\tau_\phi^{\rm plateau} \simeq 0.6 \ \ {\rm ns}/c_{\rm mag}({\rm ppm}). \tag{9}$$

TABLE V. Fit parameters for $\tau_\phi(T)$ in silver and gold samples made of our 6N sources, taking into account, on top of the contributions of electron–electron and electron–phonon interactions, the additional contribution of dilute Kondo impurities of spin-1/2 as described by Eqs. (5) and (8). The corresponding fits are displayed as continuous lines in Fig. 6.

| Sample | $A$ ($A_{\rm thy}$) ($\rm ns^{-1}\,K^{-2/3}$) | $B$ ($\rm ns^{-1}\,K^{-3}$) | $c_{\rm mag}$ (ppm) | $T_K$ (K) |
|---|---|---|---|---|
| Ag(6N)a | 0.68 (0.55) | 0.051 | 0.009 | 0.04 |
| Ag(6N)b | 0.54 (0.51) | 0.05 | 0.011 | 0.04 |
| Ag(6N)c | 0.35 (0.31) | 0.051 | 0.0024 | 0.04 |
| Ag(6N)d | 0.50 (0.47) | 0.054 | 0.012 | 0.04 |
| Au(6N) | 0.59 (0.40) | 0.08 | 0.02 | 0.01 |

Continuous lines in Fig. 5 are fits of the measured $\tau_\phi(T)$ to Eq. (5) using Eq. (8), with magnetic impurities of Kondo temperature $T_K = 40$ mK as expected for manganese atoms. The parameters $A$ and $B$ in Eq. (4) could not be extracted independently for samples Ag(5N)b, $c_{\rm Mn0.3}$, and $d_{\rm Mn1}$. To avoid increasing unnecessarily the number of fit parameters, the values of $A$ and $B$ deduced from the fit of sample Ag(6N)c (dashed line) were used. Sample Ag(6N)c was chosen as a reference because its predicted electron–electron scattering rate is close to that of samples Ag(5N)b, Ag(5N)$c_{\rm Mn0.3}$, and Ag(5N)$d_{\rm Mn1}$. Following this procedure, the measurements could be reproduced accurately with[32] $S = 1/2$ and $c_{\rm mag} = 0.13$, 0.39, and 0.96 ppm, respectively, for samples Ag(5N)b, $c_{\rm Mn0.3}$, and $d_{\rm Mn1}$, in close agreement with implanted concentrations of manganese and compatible with the nominal purity of the Saclay 5N silver source. This confirms that the effect on $\tau_\phi$ of the implantation of magnetic impurities with a low Kondo temperature is well understood, both qualitatively and quantitatively.

Looking back at the $\tau_\phi$ data for samples Ag(6N)a, b, c, d and Au(6N) shown in Fig. 4, we note that the fits to those data would also improve with the addition of a very small quantity of magnetic impurities. We performed new fits to those data using Eqs. (5) and (8), with $c_{\rm mag}$ as an additional adjustable parameter. For the silver samples we kept $T_K = 40$ mK as for manganese impurity atoms, whereas for the gold sample Au(6N) we chose $T_K = 10$ mK as for chromium impurity atoms. The values of $c_{\rm mag}$ from the fits are 0.009, 0.011, 0.0024, 0.012, and 0.02 ppm, respectively, for samples Ag(6N)a, b, c, d, and Au(6N). The new fits are shown as continuous lines in Fig. 6 and the fit parameters are given in Table V. Note that these concentrations are about 100 times smaller than the nominal total impurity concentrations of the sources. As a striking example to show how small these numbers are, 0.01 ppm of impurities in sample Ag(6N)d corresponds to about 3 impurity atoms every micrometer in the wire. Such small concentrations of Kondo impurities are essentially undetectable by any means other than measuring the phase coherence time, especially in thin films. Moreover, no commercial provider can guarantee such a high purity for the source material.

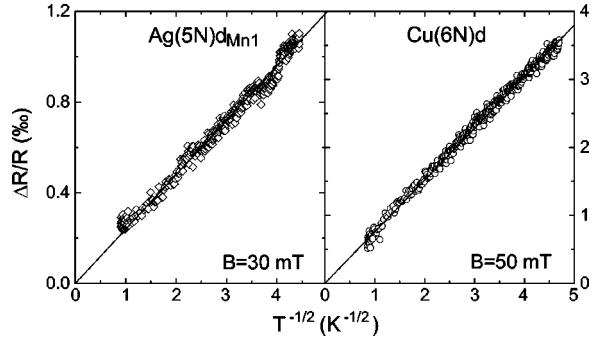


FIG. 7. Resistance of sample Ag(5N)$d_{Mn1}$ ($\diamond$) and Cu(6N)d ($\circ$) plotted as function of $1/\sqrt{T}$. Continuous lines are fits using the functional form $\Delta R(T)/R = C/\sqrt{T}$, with $C = 2.4\times10^{-4}$ (left panel) and $7.6\times10^{-4}$ $K^{1/2}$ (right panel), close to the predictions of Eq. (10) $C_{thy} = 1.8\times10^{-4}$ and $7.2\times10^{-4}$ $K^{1/2}$, respectively. The logarithmic contribution to $R(T)$ from the Kondo effect is invisible in both samples, as it is masked by the much larger contribution from electron–electron interactions in the wires. From the comparison of Figs. 5 and 7, it appears clearly that the phase coherence time is a much more sensitive probe of very dilute magnetic impurities than the temperature dependence of the resistance.

### C. Extremely dilute magnetic impurities and temperature dependence of the resistance

The temperature dependence of the resistance, $R(T)$, is often used as a probe of magnetic impurities, because of the well-known Kondo effect. Nevertheless, in thin wires, where the resistance also varies due to electron–electron interactions, it must be pointed out that $R(T)$ is not sensitive enough to detect small amounts of magnetic impurities. The contribution of electron–electron interactions,[15]

$$\frac{\Delta R(T)}{R} \simeq 3.126 \frac{R}{R_K}\frac{L_T}{L} \equiv \frac{C_{\rm thy}}{\sqrt{T}}, \tag{10}$$

with $L_T = \sqrt{\hbar D/k_B T}$ the thermal length, is much stronger and varies much more rapidly with temperature than the Kondo term, determined by $\Delta\rho_{\rm Kondo} \simeq -B_K \ln(T)$,[33] where $B_K \approx 0.2$ n$\Omega$ cm/ppm.[34] In our wires where the resistivity is about $\rho \sim 3$ $\mu\Omega$ cm, the corresponding relative variation of the resistance is about $10^{-5}$ per decade of temperature for 1 ppm of Kondo impurities. This is more than an order of magnitude smaller than the typical contribution of electron–electron interactions between 100 mK and 1 K.

This is illustrated in the left panel of Fig. 7 with sample Ag(5N)$d_{Mn1}$ in which we implanted 1 ppm of manganese. The resistances are measured in a magnetic field $B \sim 20$–$50$ mT, large enough to suppress the WL corrections but small enough to avoid freezing out the spin–flip scattering of conduction electrons by magnetic impurities. We checked on several samples showing anomalous dephasing that $R(T)$ is independent of the applied magnetic field.

A striking conclusion is that the phase coherence time is a much more sensitive probe of very dilute magnetic impurities than the temperature dependence of the resistance, which is dominated by electron–electron interactions at low temperature.

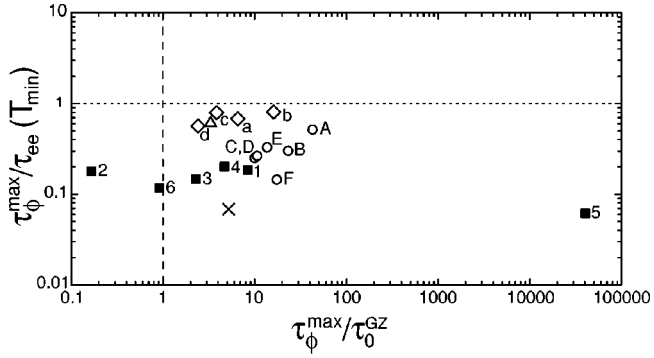


FIG. 8. Comparison between the predictive powers of the conventional theory of electron–electron interactions (Ref. 3), and of the theory of Golubev and Zaikin (Refs. 23,35). The $X$ coordinate gives the ratio of the phase coherence time measured at the lowest temperature, $\tau_\phi^{\rm max}$, to $\tau_0^{\rm GZ}$, calculated from Eq. (11) with $b = 1$. The $Y$ coordinate is the ratio of $\tau_\phi^{\rm max}$ to $\tau_{ee}(T_{\rm min})$, the value calculated using the conventional theory [Eq. (3)] at the lowest temperature $T_{\rm min}$. Open symbols are data points for which the phase coherence time continues to increase at the lowest measurement temperature. Full symbols and $\times$ are data points for which the phase coherence time is nearly constant at low temperature. The conventional theory predicts that all data points lie on the horizontal dotted line if no extrinsic degrees of freedom, such as magnetic impurities, limit the phase coherence time. The GZ theory predicts that all data points lie on a vertical line if the phase coherence time already saturates, and to the left of that line if $\tau_\phi$ still increases at low temperature. (The dashed line corresponds to the case $b = 1$ in the GZ theory.)

## VI. OTHER EXPLANATIONS OF ANOMALOUS DEPHASING

The evidence presented in the previous section shows that very dilute magnetic impurities could explain the anomalous dephasing frequently observed at low temperature. But are there other viable explanations?

### A. Dephasing by high energy electromagnetic modes

Golubev and Zaikin (GZ) proposed[23,35] that zero temperature dephasing by high energy electromagnetic modes is responsible for the frequently observed saturation of $\tau_\phi$ in metallic thin films. This theory, which is controversial,[36] predicts that the phase coherence time saturates at low temperature at $\tau_0^{\rm GZ}$ given by[35]

$$\frac{1}{\tau_0^{\rm GZ}} = \frac{\sqrt{2}\rho}{3R_K\pi\sqrt{D}}\left(\frac{b}{\tau_e}\right)^{3/2}, \tag{11}$$

where $b$ is a constant numerical factor expected to be of order 1. It is interesting to point out that for a given material $\tau_0^{\rm GZ}$ is proportional to $D^3$ and is insensitive to the actual geometry of the sample.

Using this prediction, GZ were able to account for a subset of the experimental results published in Refs. 24,37 using the overall prefactor of the dephasing rate as an adjustable parameter.[35] Note that, as explained by GZ in their latest article,[35] the comparison with MJW data performed in Ref. 38 should be ignored because it was done using an expres-

sion for $\tau_0^{GZ}$ that does not apply to the experiment, but is valid only when the elastic mean free path exceeds the transverse dimensions of the wires.

Since the exact prefactor is unknown, it is not possible to rule out this theory by comparison with a single experiment. Instead, we propose here to compare the predictive power of the GZ theory with the conventional theory of electron–electron interactions for many samples. This is done in Fig. 8. This figure includes all gold, silver and gold–palladium samples for which it has not been shown that magnetic impurities are the main source of decoherence at low temperature, plus sample Cu(5N)a which was used by GZ for comparison of their theory with experiments.[35] (We do not show other copper samples or samples made from our 5N silver source, because they clearly contain magnetic impurities. See Sec. VII and Ref. 39.) The $X$ coordinate in Fig. 8 gives the ratio of the phase coherence time measured at the lowest temperature, $\tau_\phi^{max}$, to $\tau_0^{GZ}$, calculated from Eq. (11) with $b=1$. The $Y$ coordinate is the ratio of $\tau_\phi^{max}$ to $\tau_{ee}(T_{min})$, the value calculated using the conventional theory [Eq. (3)] at the lowest temperature $T_{min}$. Open symbols are samples for which $\tau_\phi$ continues to increase at the lowest measurement temperature; upon cooling they move to the right. Full symbols are samples for which $\tau_\phi$ is nearly constant at low temperature; they move downward when the temperature is reduced. As for theory, GZ predict that all full symbols should be aligned on a vertical line $\tau_\phi^{max}/\tau_0^{GZ}=b^{3/2}$, whereas open symbols would be located at $\tau_\phi^{max}/\tau_0^{GZ}<b^{3/2}$. In contrast, the conventional theory predicts that all data points should be aligned on the horizontal line $\tau_\phi^{max}/\tau_{ee}(T_{min})=1$. On this plot the data scatter in both directions. The most salient feature of the plot, however, is that the scatter in the horizontal direction extends over more than five orders of magnitude, whereas the scatter in the vertical direction extends over slightly more than one decade. The horizontal scatter indicates that GZ theory does not reproduce the dependence of $\tau_\phi$ on sample parameters. In particular, the GZ prediction depends much too strongly on the diffusion coefficient, which varies considerably in MJW's six gold samples.

While no theory explains all of the experimental data without any additional parameters, it appears that the conventional theory does a better job than the GZ theory to predict the low temperature value of $\tau_\phi$.

### B. Dephasing by two level systems

Two approaches to electron dephasing by two-level tunneling systems (TLS) have been proposed. The first, by Imry, Fukuyama, and Schwab,[21] requires a nonstandard distribution of TLS parameters. It was shown later that such a distribution would lead to large anomalies in the low-temperature specific heat, and in acoustic attenuation at very low temperature.[40] The second approach describes the coupling between the conduction electrons and the TLS via the two-channel Kondo effect.[22] In this model, the effect of TLS is very similar to that of magnetic impurities in the Kondo regime, at least at $T \gtrsim T_K$. The main criticism raised against this explanation is that, starting from any realistic model of a TLS, it may be impossible to reach the strong coupling regime where the Kondo temperature is larger than the tunneling level splitting.[41,42] From the experimental point of view, measurements of $\tau_\phi$ from the weak localization contribution to the magnetoresistance cannot discriminate between magnetic impurities and TLS.

## VII. TEST OF THE MAGNETIC IMPURITY HYPOTHESIS: PROBING $\tau_\phi(B)$

A definitive test of the role of spin-flip scattering for the saturation of $\tau_\phi$ at low temperature is to probe how the dephasing time depends on magnetic field. It is expected that spin–flip scattering is suppressed when the dynamics of magnetic impurities is frozen by application of a sufficiently large magnetic field $B$. Indeed, if the Zeeman splitting is much larger than $k_BT$, magnetic impurities stay in their ground state. As a result spin–flip collisions vanish and $\tau_\phi$ should climb up to the value expected from electron–electron interactions (independent of $B$ as long as the cyclotron radius is much larger than the elastic mean free path). In the presence of spin-1/2 impurities, and neglecting Kondo effect, the spin–flip scattering rate of electrons vanishes at large field as (see Appendix C and Ref. 43)

$$\frac{\tau_{sf}(B=0)}{\tau_{sf}(B)}=\frac{g\mu B/k_BT}{\sinh(g\mu B/k_BT)}, \tag{12}$$

where $g$ is the renormalized gyromagnetic factor of the magnetic impurities.

One possible method to detect a variation in $\tau_\phi$ with magnetic field is to measure the average amplitude $\Delta G_{UCF}$ of universal conductance fluctuations in a metallic wire as a function of magnetic field. This method has two drawbacks. First $\Delta G_{UCF} \propto \tau_\phi^{1/4}$ depends only weakly on the phase coherence time. Second the large correlation field $\Delta B_{UCF} \simeq h/(ewL_\phi)$ of conductance fluctuations in mesoscopic wires makes it difficult to obtain accurate estimates of the averaged $\Delta G_{UCF}(B)$ at low temperature in the field range below the relevant magnetic field scale $g\mu B \sim k_BT$. For example, in Cu(6N)b, $\Delta B_{UCF} \simeq 25$ mT at 40 mK, whereas the characteristic field needed to freeze the magnetic impurities is as low as $k_BT/2\mu \simeq 55$ mT.

We have chosen instead to probe the magnetic field dependence of $\tau_\phi$ by measuring the Aharonov-Bohm (AB) oscillations in the magnetoresistance of ring-shaped samples. For this purpose, we have fabricated two copper rings of radius $r=0.5$ and 0.75 $\mu$m, respectively, on the same chip as samples Cu(6N)c and Cu(6N)d. The ring perimeters are chosen to be larger than or similar to the phase coherence length at $B \approx 0$ in order to increase the sensitivity to variations of $\tau_\phi$. The averaged $h/e$ AB oscillations amplitude $\Delta G_{AB}$ is related to the phase coherence time through[44]

$$\Delta G_{AB}=C\frac{e^2}{h}\frac{L_T}{\pi r}\sqrt{\frac{L_\phi}{\pi r}}\exp\left[-\frac{\pi r}{L_\phi}\right], \tag{13}$$

where $C$ is a geometrical factor of order 1. The short period of AB oscillations with B (5.5 and 2.5 mT for $r=0.5$ and 0.75 $\mu$m, respectively) allows to estimate accurately the

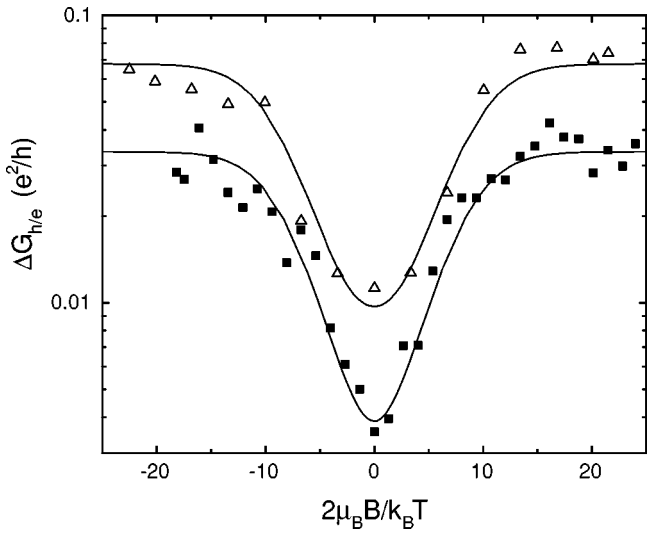


FIG. 9. Symbols: mean amplitude of the AB $h/e$ oscillations ($\Delta G_{h/e}$) across the ring in sample Cu(6N)d at $T=40$ (△) and 100 mK (■), plotted in units of $e^2/h$ as a function of the reduced magnetic field $2\mu_B B/k_B T$. Solid lines: fits to the two data sets using Eqs. (5), (12), and (13) with $C$ and $g$ as fit parameters. At 40 mK, the AB oscillations are unmeasurably small at B=0; the fit to those data includes the noise floor of the experiment.

magnetic field dependence of $\Delta G_{\mathrm{AB}}$ on the much larger field scale needed to freeze the magnetic impurities.

This experiment was performed on copper samples because it is the material in which the presence of magnetic impurity was most questionable: no correlations were found between $\tau_\phi$ and the copper source material purity; moreover, whereas in some samples $\tau_\phi$ saturates at values as small as 0.2 ns [3 times smaller than in $\mathrm{Ag(5N)d_{Mn1}}$] we observed neither a nonmonotonic temperature dependence of $\tau_\phi(T)$, as in $\mathrm{Ag(5N)d_{Mn1}}$ (see Fig. 5), nor a Kondo contribution to $R(T)$.

Our experimental procedure and data analysis are detailed in Ref. 25. Figure 9 shows the amplitude of AB oscillations measured across the ring in sample Cu(6N)d at $T=40$ and 100 mK (symbols) as a function of reduced magnetic field $2\mu B/k_B T$. The data in Fig. 9 show that the amplitude of AB oscillations increases with magnetic field by a factor 8 at 100 mK and a factor 7 at 40 mK,[45] on a characteristic field scale proportional to $T$.

The solid lines in Fig. 9 are fits to the simple model represented by Eqs. (12) and (13), explained in Appendix C. We assumed that $\tau_\phi$ at large $B$ is limited only by electron–electron interactions and used the values given by theoretical prediction [Eq. (3)]: $\tau_\phi=5.4$ and 9.9 ns at 100 and 40 mK, respectively. The two remaining parameters, namely the gyromagnetic factor $g$ and the geometrical constant[46] $C$, were adjusted to reproduce accurately our data. The best fit is obtained with $g=1.08$ and $C=0.17$. Note that a more rigorous approach to the magnetic-field dependence of AB oscillation amplitude has been published recently by Vavilov and Glazman.[47] Using their prediction [Eqs. (62) and (63) in Ref. 47] with a magnetic impurity spin[48] $S=1/2$ and $g=0.90$, we obtain a fit indistinguishable from the solid lines calculated with the simple model.

The impurity $g$-factors obtained from these fits, 1.08 and 0.90, are small, like the value $g=1.36$ found for electrons by neutron scattering in bulk CuO.[49]

This set of experiments confirms that spin–flip collisions are responsible for the apparent low temperature saturation of $\tau_\phi$ we observe in copper samples.

## VIII. COMPARISON WITH ENERGY EXCHANGE MEASUREMENTS

Parallel to this work, a systematic correlation was found between dephasing and energy exchange between electrons: all samples made of the same source material, using the same deposition system, either followed the theory of electron–electron interactions for both energy exchange and phase coherence, or displayed anomalous behaviors for both phenomena.[11,24,50,51] This correlation suggests that magnetic impurities could also be responsible for anomalous energy exchange. Such a possibility had not been considered until recently because, all spin states being degenerate at zero magnetic field, magnetic impurities do not contribute to energy exchange in first order. However, Kaminsky and Glazman have pointed out that energy exchange in the presence of magnetic impurities may take place with an appreciable efficiency by a second-order process.[52] The experimental proof that excess energy exchange observed in samples made of the 5N silver and copper sources results from dilute paramagnetic spins was obtained recently by measuring the dependence of energy exchange upon magnetic field.[39] Similarly to what was observed on the dephasing rate, the application of a large magnetic field on these samples reduces the rate of energy exchange. Note however that the amount of magnetic impurities needed to account for the measured energy exchange rates seems to be significantly larger than the estimations from $\tau_\phi(T)$; in the case of copper, the obtained $g$-factor $g=2.3$ is also different. More experiments are needed to clarify these issues.

## IX. CONCLUSION

By measuring the phase coherence time as a function of temperature on wires made of silver, gold, and copper, from source materials of different purities, we have found that anomalous dephasing is correlated to source material purity in silver and gold samples, and systematic in copper samples. We showed experimentally that the presence of very dilute magnetic impurities with a low Kondo temperature in the host material can result in a broad plateau in $\tau_\phi(T)$ while being undetected in the temperature dependence of the resistance. Measurement of the magnetic field dependence of Aharonov-Bohm oscillations on relatively large copper rings revealed that the phase coherence time increases with $B$ on a field scale proportional to the temperature. This confirms that an apparent ''saturation'' of $\tau_\phi$ can be attributed to very dilute magnetic impurities.[53]

In the silver and gold samples discussed in this paper, we impute the presence of magnetic impurities to the purity of the material sources. We found that large coherence times at 40 mK could be obtained in samples fabricated with the

silver sources of the highest purity commercially available (6N). However, it is very difficult to rule out a small contamination during the evaporation process and eventually sample preparation. In the case of copper, the Kondo impurities probably originate from the copper oxide at the surface.[26]


## ACKNOWLEDGMENTS

This work was supported by NSF Grants Nos. DMR-9801841 and 0104178, and by the Keck Microfabrication Facility supported by NSF DMR-9809688. We acknowledge the assistance of S. Gautrot, O. Kaitasov, and J. Chaumont at the CSNSM in Orsay University, who performed the ion implantation in samples $Ag(5N)c_{Mn0.3}$ and $Ag(5N)d_{Mn1}$. We are grateful to I. Aleiner, B.L. Altshuler, H. Bouchiat, M.H. Devoret, V.I. Fal'ko, L.I. Glazman, D. Natelson, M.G. Vavilov, and A.D. Zaikin for interesting discussions.


## APPENDIX A: ELECTRON COOLING IN TRANSPORT MEASUREMENTS AT LOW TEMPERATURES

Joule heating is a concern when transport measurements are performed at low temperatures. Any current results in the production of heat, which can be either transferred directly to the phonons in the wire, or to the electrons in the contact pads, assumed to be much larger than the wire. At sub-Kelvin temperatures, the first process becomes very inefficient. The reason is that the phonon emission rate for an electron with an excess energy $k_BT$ goes like[11] $\gamma \simeq 5\kappa_{ph}(k_BT)^3$, with $\kappa_{ph} \simeq 10\ \mathrm{ns}^{-1}\,\mathrm{meV}^{-3}$. The distance it will travel before losing its extra energy is then $\sqrt{D/\gamma} \simeq 18\ \mu\mathrm{m} \times (T/1\ \mathrm{K})^{-3/2}$ for a typical diffusion coefficient $D = 100\ \mathrm{cm}^2/\mathrm{s}$. At $T = 40$ mK, $\sqrt{D/\gamma} \simeq 2.2$ mm, a very macroscopic distance! Therefore one must take care that the electron's energy never gets so large at low temperature. Taken alone, the cooling by the contact pads through electronic heat transport results in a temperature profile in the wire

$$T_e(x) = \sqrt{T^2 + \frac{3}{\pi^2}x(1-x)\left(\frac{eV}{k_B}\right)^2}, \qquad \text{(A1)}$$

with $T_e$ the electron temperature in the contacts placed at the ends of the wire, assumed to be equal to the temperature of the phonons, $x$ the relative position along the wire, and $V$ the voltage across the wire. For $T = 0$, the maximum temperature is $(\sqrt{3}/2\pi)(eV/k_B) \approx 3.2\ \mathrm{K} \times V/(1\ \mathrm{mV})$. By limiting the voltage across the sample to $eV = k_BT$, the maximal electron temperature is $T\sqrt{1 + (3/4\pi^2)} \simeq 1.04\ T$. With such a low applied voltage, the phase coherence time, supposed to increase as $T_e^{-2/3}$ at low temperature, varies through the sample by $1 - 1.04^{-2/3} \simeq 2\%$, which is sufficiently small for most purposes. However, at very low temperature, a measurement of a voltage of order $k_BT/e$ might become very time consuming if one considers that the input voltage noise for the best room-temperature commercial amplifiers is about $1\ \mathrm{nV}/\sqrt{\mathrm{Hz}}$ and that the weak localization correction to the conductance is about $10^{-3}$ of the total signal. For example at 10 mK, $10^{-3}k_BT/e \simeq 1$ nV, and an integration time of 100 s for each conductance measurement is needed to get a signal to noise ratio of 10. In fact, this estimation is often too pessimistic because cooling by phonons does play a role for long wires.[54] In order to evaluate this effect precisely, one has to solve the complete heat equation, which can be written in reduced units ($t_e(x) = T_e(x)/T$, $v = eV/k_BT$),

$$v^2 + \frac{\pi^2}{6}\frac{d^2}{dx^2}t_e^2(x) - \left(\frac{T}{T_{co}}\right)^3 (t_e^5(x) - 1) = 0, \qquad \text{(A2)}$$

in which the first term describes Joule heating, the second the thermal conductivity of electrons, assuming Wiedemann-Franz law, and the last one the coupling to phonons.[11,55] We have defined a crossover temperature

$$T_{co} = (\Sigma \rho L^2 (e/k_B)^2)^{-1/3}, \qquad \text{(A3)}$$

with $L$ the length of the wire, $\rho$ its resistivity, $\Sigma$ the electron–phonon coupling constant[56] (typically $\Sigma \sim 1$–$10\ \mathrm{nW}/\mu\mathrm{m}^3/\mathrm{K}^5$ in metallic thin films on Si substrate). The resulting temperature profile is shown in Fig. 10 for typical values: we consider a silver wire ($\Sigma \simeq 3\ \mathrm{nW}/\mu\mathrm{m}^3/\mathrm{K}^5$ from Table III) with $D = 100\ \mathrm{cm}^2/\mathrm{s}$, $L = 0.2$ mm, at $T = 100$ and 200 mK, for $eV/k_BT = 3$. The dotted line indicates the solution without phonons, the dashed line the solution without electronic heat transport. For this set of parameters, the crossover temperature is $T_{co} \simeq 120$ mK. Hence, at 200 mK phonons reduce significantly the maximum electron temperature, which does not exceed the bath temperature by more than 16%. At 100 mK, cooling by phonon emission is inefficient, and the maximum electron temperature is 27% above $T$.

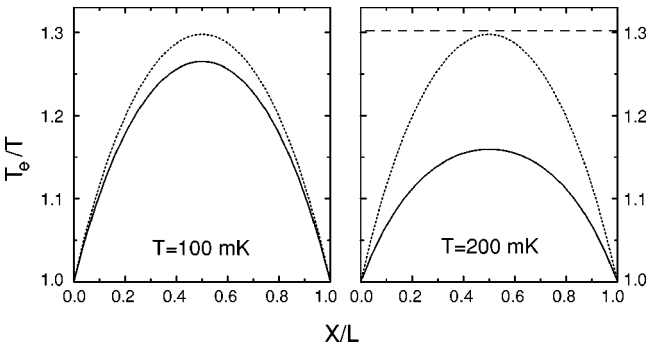


FIG. 10. Electrons heating in a typical silver wire (see text) of length $L = 0.2$ mm, biased with a dc voltage $V$ such that $eV/k_BT = 3$ and for phonon temperatures $T = 100$ and 200 mK, respectively, in the left and right panel. Continuous lines: ratio of electron temperature $T_e$ with phonon temperature as function of the reduced position $X/L$ in the wire, taking into account electron–phonon interactions [see Eq. (A2)]. Dotted lines: electron temperature as function of position neglecting phonons [see Eq. (A1)]. Dashed line in the right panel: electron temperature neglecting electronic heat transport (in the left panel this line would stand at $T_e/T = 1.87$).

The analysis of the exact solutions of this equation allows to distinguish two opposite regimes: for $T \ll T_{co}$, electrons are decoupled from phonons (cooling by phonons will become active only if the applied voltage is so high that the maximal temperature is above $T_{co}$), and temperature is given

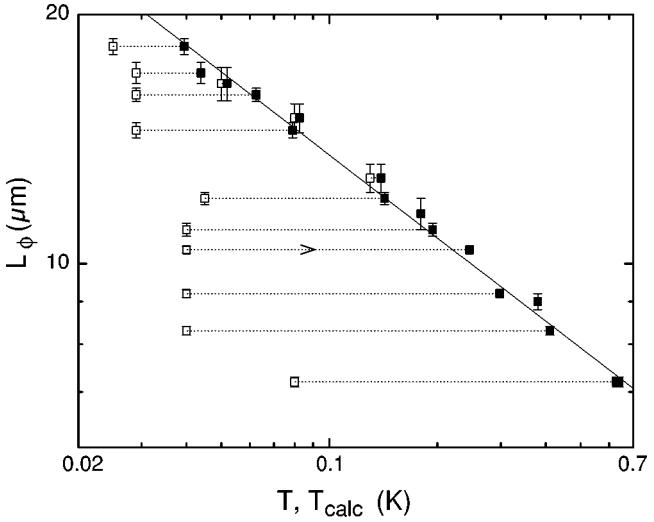


FIG. 11. Full symbols: phase coherence length measured on a 6N silver sample as a function of the electronic temperature $T_{\rm calc}$ calculated using Eq. (A2) for a cryostat temperature $T$ represented by the attached open symbol. The continuous line represents the theoretical prediction $L_\phi \propto T^{-1/3}$ of electron–electron interactions (data taken at Saclay).

by the electronic conductivity alone, see Eq. (A1). This is the difficult regime, where the maximal voltage is of the order of $k_BT/e$. In the opposite situation $T \gg T_{\rm co}$, heat transfer to the contacts can be neglected, and cooling by phonons rules the game. The temperature of the electrons is then nearly homogeneous, with $T_e/T \approx (1+(T_{\rm co}/T)^3 v^2)^{1/5}$ and for $(T_{\rm co}/T)^3 v^2 \ll 1$ the temperature does not exceed $T$ excessively: $T_e \approx T + \frac{1}{5}[T_{\rm co}^3 (eV/k_B)^2/T^4]$. One should thus fabricate wires as long as possible, in order to have a small crossover temperature $T_{\rm co}$ which allows to work at larger voltages.

In order to test the validity of this calculation, we performed a control experiment in which electrons were intentionally heated by applying ac currents. The sample, similar to the others presented in this review, consists of a 1.79-mm-long, 150-nm-wide, and 45-nm-thick wire made out of a 6N purity silver source. The diffusion coefficient $D = 139\ {\rm cm}^2/{\rm s}$ results in a crossover temperature $T_{\rm co} = 30$ mK. We extracted the phase coherence length $L_\phi$ from the magnetoresistance. For each magnetoresistance trace we show in Fig. 11 two symbols, one open and one full, at a *Y*-coordinate given by the corresponding value of $L_\phi$. Open symbols are at the *X*-coordinate given by the cryostat temperature $T$ at which the measurement was performed, whereas full symbols are at the *X*-coordinate given by the calculated electron temperature $T_{\rm calc}$. Since the magnetoresistance is given by $L_\phi \propto T^{-1/3}$, $T_{\rm calc}$ was calculated from the time- and position-average of $T_e^{-1/3}$, using temperature profiles obtained with Eq. (A2). For example, the pair of data points at $L_\phi \simeq 10.4\ \mu$m corresponds to $T = 40$ mK, $V_{\rm ac} = 0.86$ mV rms, leading to $T_{\rm calc} = 245$ mK. The data points with large heating ($T_{\rm calc} \gg T$) as well as those with little heating ($T_{\rm calc} \simeq T$) fall close to a single line $L_\phi \propto T^{-1/3}$, indicating that the electron temperature is correctly modeled.

## APPENDIX B: DEPHASING BY ELECTRON–ELECTRON INTERACTIONS

Assuming that we can restrict ourself to two body interactions, the dephasing rate, or inverse lifetime, $1/\tau_{\rm in}(E,T)$ of an electron at energy $E$ coupled only to the electronic fluid at temperature $T$ results from all collision processes allowed by the Pauli exclusion principle,

$$\tau_{\rm in}^{-1}(E,T) \simeq \int_{|\varepsilon| \gtrsim \hbar/\tau_\phi} d\varepsilon \;\; K(\varepsilon)(1-f_T(E-\varepsilon))h(\varepsilon,T), \tag{B1}$$

where $f_T(E)$ is the Fermi function at temperature $T$, $K(\varepsilon)$ is the interaction "Kernel" of the screened Coulomb interaction, proportional to the modulus square of the interaction matrix element for an exchanged energy $\varepsilon$, and

$$h(\varepsilon,T) = \int_{-\infty}^{\infty} dE' f_T(E')(1-f_T(E'+\varepsilon))$$

$$= \frac{\varepsilon}{1-\exp(-\varepsilon/k_BT)}. \tag{B2}$$

The low energy cut-off $|\varepsilon| \gtrsim \hbar/\tau_\phi$ in Eq. (B1) is introduced because fluctuations on time scales longer than the electron's lifetime can be considered as static.[4]

The interaction kernel $K(\varepsilon)$ depends only on $\varepsilon$ since the energies of interacting electrons are close to the Fermi energy $E_F$ and $\varepsilon \lesssim k_BT \ll E_F$. Our samples are quasi-1D because the width and thickness of the wires are smaller than the length $L_\varepsilon = \sqrt{\hbar D/\varepsilon}$ for the probed energy exchanged. For quasi-1D samples the interaction kernel reads[57]

$$K(\varepsilon) = \kappa |\varepsilon|^{-3/2}, \tag{B3}$$

with

$$\kappa^{-1} = \hbar \sqrt{\frac{\pi \nu_F S L}{4} \frac{R_K}{R}}. \tag{B4}$$

The dephasing rate $1/\tau_{ee}(T)$ is the inverse lifetime averaged over thermal excitations

$$1/\tau_{ee}(T) = \int dE \frac{f_T(E)(1-f_T(E))}{k_BT} \tau_{\rm in}^{-1}(E,T). \tag{B5}$$

Injecting Eqs. (B1) and (B3) into Eq. (B5) we obtain[58]

$$1/\tau_{ee}(T) \simeq \int_{\hbar/\tau_{ee}}^{\infty} d\varepsilon \frac{\kappa\sqrt{\varepsilon}}{k_BT} \frac{\exp(\varepsilon/k_BT)}{(1-\exp(\varepsilon/k_BT))^2}. \tag{B6}$$

This expression shows that the effect of electron–electron interactions on quantum coherence in mesoscopic wires is dominated by processes with a small exchanged energy $\varepsilon \approx \hbar/\tau_\phi$. It is interesting to point out that this implies that a sample is quasi-1D with respect to decoherence as long as the phase coherence length $L_\phi = \sqrt{D\tau_\phi}$ is large compared to its transverse dimensions and small compared to its length.

This is not true for energy exchange, for which the dimensionality is determined by the length associated with the largest exchanged energy.

In order to obtain an analytical expression for $\tau_{ee}(T)$ we make the following approximation:

$$\frac{\exp(\varepsilon/k_BT)}{(1-\exp(\varepsilon/k_BT))^2} \simeq \frac{1}{(\varepsilon/k_BT)^2}. \tag{B7}$$

This approximation is justified since the integral is dominated by small energy exchanges. This leads to

$$\tau_{ee} \simeq \hbar \left[ \frac{(\pi/16)(R_K/R)\nu_F SL}{(k_BT)^2} \right]^{1/3}, \tag{B8}$$

where we used Eq. (B4) for the interaction kernel.

The calculation of $\tau_\phi$ described above makes use of a low energy cut-off, therefore the prefactor in Eq. (B8) is not reliable. To solve this technical difficulty, Altshuler, Aronov, and Khmelnitsky[3] calculated the effect of electron–electron interactions through the interaction of one electron with the fluctuating electromagnetic field resulting from other electrons at thermal equilibrium. Within this approach it is possible to calculate directly the conductivity taking into account electron–electron interactions. The dephasing rate is then obtained without reference to the energy decay rate. Neglecting spin–orbit coupling, this calculation yields[15]

$$\frac{\Delta R}{R}(B,T) = -\frac{2R}{R_K}\frac{\sqrt{D\tau_N}}{L}\frac{\mathrm{Ai}(\tau_N/\tau_H)}{\mathrm{Ai}'(\tau_N/\tau_H)}, \tag{B9}$$

with

$$\tau_N = \hbar \left[ \frac{(R_K/R)\nu_F SL}{2\pi(k_BT)^2} \right]^{1/3},$$

$$\tau_H = \frac{3\nu e^2 RS}{L}\left(\frac{\phi_0}{2\pi wB}\right)^2,$$

where $\phi_0 = h/e \simeq 4.1\times 10^{-15}\ \mathrm{T\,m^2}$ is the flux quantum, $\mathrm{Ai}(x)$ is the Airy function and $\mathrm{Ai}'(x)$ its derivative. The time $\tau_N$ is often called Nyquist time in reference to the fluctuation-dissipation theorem used to evaluate the electromagnetic fluctuations for the calculation of weak localization corrections.

Since expression (B9) includes electron–electron interactions, it should be possible to deduce the contribution $\tau_{ee}$ of the screened Coulomb interaction on the phase coherence time. This can be done by pointing out that

$$\frac{\mathrm{Ai}(x)}{\mathrm{Ai}'(x)} = \frac{-1}{\sqrt{1/2+x}}(1+\epsilon(x)), \tag{B10}$$

where $|\epsilon(x)|<0.04$ for $x>0$. In practice, the experimental resolution is not sufficient to distinguish a relative discrepancy smaller than 4% of the amplitude of weak localization corrections, which are themselves smaller than 1% of the measured signal. Hence we can write

$$\frac{\Delta R}{R}(B,T) = \frac{2R}{R_K L}\sqrt{\frac{D}{1/2\tau_N + 1/\tau_H}}. \tag{B11}$$

A comparison with Eq. (1) (neglecting spin–orbit coupling) allows us to extract the phase coherence time when it is limited by electron–electron interactions,

$$\tau_{ee} = \hbar \left[ \frac{(4/\pi)(R_K/R)\nu_F SL}{(k_BT)^2} \right]^{1/3}$$

$$= 2\tau_N. \tag{B12}$$

This expression of the phase coherence time $\tau_{ee}$ is larger by a factor $4/\pi^{2/3} \simeq 1.9$ than the cut-off-dependent estimation in Eq. (B8).

## APPENDIX C: MAGNETIC FIELD DEPENDENCE OF SPIN–FLIP SCATTERING

This appendix present a simple calculation of electron spin-flip scattering from magnetic impurities as a function of applied magnetic field $B$. The calculation is carried out at first order in spin–flip scattering, neglecting the Kondo effect. Moreover we consider here, for simplicity, magnetic impurities of spin-1/2.

The spin–flip rate $\tau_{\mathrm{sf}}^{-1}(E,B)$ of an electron at energy $E$ is obtained from the Fermi Golden Rule,

$$\tau_{\mathrm{sf}}^{-1}(E,B) = c_{\mathrm{mag}}\lambda\{P_-(1-f_T(E-g\mu B)) + P_+(1-f_T(E+g\mu B))\}, \tag{C1}$$

where $c_{\mathrm{mag}}$ is the concentration of magnetic impurities, $\lambda$ is proportional to the modulus square of the interaction potential electron-magnetic impurity, and $P_\pm$ is the probability to have the magnetic impurity in the up $(+)$ or down $(-)$ state relative to the magnetic field direction $B$. In absence of Kondo effect $\lambda$ is approximated as independent of energy and magnetic field.

Since at thermal equilibrium $P_\pm = f_T(\pm g\mu B)$, we obtain

$$\tau_{\mathrm{sf}}^{-1}(E,B) = \frac{c_{\mathrm{mag}}\lambda(1+\exp(E/k_BT))/2}{\cosh(E/k_BT)+\cosh(g\mu B/k_BT)}. \tag{C2}$$

The spin–flip rate $\tau_{\mathrm{sf}}^{-1}(B)$ is averaged over electronic excitations

$$\tau_{\mathrm{sf}}^{-1}(B) = \int_{-\infty}^{+\infty} dE \frac{f_T(E)(1-f_T(E))}{k_BT}\tau_{\mathrm{sf}}^{-1}(E,B),$$

which gives

$$\frac{\tau_{\mathrm{sf}}(B=0)}{\tau_{\mathrm{sf}}(B)} = \frac{g\mu B/k_BT}{\sinh(g\mu B/k_BT)}. \tag{C3}$$

This result, also given in Ref. 43, is a finite-temperature generalization of the expression used by Benoit *et al.*[59] A rigorous theoretical calculation of the Aharonov-Bohm oscillation amplitude $\Delta G_{h/e}$ in presence of magnetic impurities

under a large externally applied magnetic field was first presented by Fal'ko.[60] A complete derivation of the magnetic field dependence of $\Delta G_{h/e}$ from first principles was finally published recently by Vavilov and Glazman.[47] As discussed in Sec. VII, the Vavilov-Glazman crossover function for $S=1/2$ is nearly indistinguishable from ours.

*Email address: fred.pierre@laposte.net. Permanent address after January 1, 2004: Laboratoire de Photonique et de Nanostructures (LPN)-CNRS, Route de Nozay, 91460 Marcoussis, France.

†Present address: Center for Advanced Nanotechnolgy, University of Toronto, Toronto, Ontario M5S 3E3, Canada.

[1] For a review, see *Mesoscopic Phenomena in Solids*, edited by B.L. Altshuler, P.A. Lee, and R.A. Webb (Elsevier, Amsterdam, 1991).

[2] A. Schmid, Z. Phys. **259**, 421 (1973).

[3] B.L. Altshuler, A.G. Aronov, and D.E. Khmelnitsky, J. Phys. C **15**, 7367 (1982).

[4] B.L. Altshuler and A.G. Aronov, in *Electron–Electron Interactions in Disordered Systems*, edited by A.L. Efros and M. Pollak (Elsevier Science, Amsterdam, 1985).

[5] S. Wind, M.J. Rooks, V. Chandrasekhar, and D.E. Prober, Phys. Rev. Lett. **57**, 633 (1986).

[6] P.M. Echternach, M.E. Gershenson, H.M. Bozler, A.L. Bogdanov, and B. Nilsson, Phys. Rev. B **48**, 11 516 (1993).

[7] P. Mohanty, E.M.Q. Jariwala, and R.A. Webb, Phys. Rev. Lett. **78**, 3366 (1997).

[8] H. Pothier, S. Guéron, N.O. Birge, D. Esteve, and M.H. Devoret, Phys. Rev. Lett. **79**, 3490 (1997).

[9] Some of the measurements shown in this article have already been published elsewhere (Refs. 11,24,25,50). (A list of samples with cross-references to previous articles is given in Ref. 14.)

[10] We did not need to perform ion-etching of the surface (Ref. 7) or predeposition of another metallic layer to promote the adhesion of the films.

[11] F. Pierre, Ann. Phys. (Paris) **26**, No. 4 (2001).

[12] For most samples we first melt the source material, evaporate 10–20 nm with a shutter protecting the sample, and pump down the chamber again for about 15 mn before the actual deposition. This pre-evaporation covers the walls of the evaporator with a clean layer of metal and makes it possible to maintain the pressure below $10^{-6}$ mbar during material deposition. We did not notice a reproducible difference between samples for which we did or did not follow this procedure.

[13] G. Bergmann, Phys. Rep. **107**, 1 (1984); S. Chakravarty and A. Schmid, *ibid.* **140**, 19 (1986).

[14] Ag(6N)a is Ag in Ref. 24, and Ag1 in Ref. 11. Ag6N(b) is Ag2 in Ref. 11. Au(6N) is AuMSU in Refs. 11,50. Cu(6N)a to Cu(6N)d are Cu1 to Cu4 in Ref. 25. Cu(5N)a is Cu in Ref. 24, and Cu1 in Ref. 11. Cu(5N)b is Cu2 in Ref. 11.

[15] I.L. Aleiner, B.L. Altshuler, and M.E. Gershenson, Waves Random Media **9**, 201 (1999).

[16] B.L. Altshuler and A.G. Aronov, Pis'ma Zh. Eksp. Teor. Fiz. **33**, 515 (1981) [JETP Lett. **33**, 499 (1981)].

[17] Several explanations can account for the small difference, mostly observed on silver samples, between the width measured using an electronic microscope and the one used to make accurate fits of low field magnetoresistance with weak localization theory. Amongst them we point out the non-uniformity of our wires, our limited accuracy on the average width (about $\pm 5$ nm), the fact we assume a rectangular section for the wires, and most likely the limit of the diffusive approximation in silver wires for which the elastic mean free path is not always very small compared to $w$ and which exhibit visible grain structure.

[18] Samples made of our 4N gold source also display anomalous dephasing. However, we could detect in these samples the presence of about 50 ppm of magnetic impurities, probably iron, that explains the observed temperature dependence of $\tau_\phi$. For details, see Ref. 50.

[19] B.L. Altshuler, M.E. Gershenson, and I.L. Aleiner, Physica E (Amsterdam) **3**, 58 (1998).

[20] S. Hikami, A.I. Larkin, and Y. Nagaoka, Prog. Theor. Phys. **63**, 707 (1980).

[21] Y. Imry, H. Fukuyama, and P. Schwab, Europhys. Lett. **47**, 608 (1999).

[22] A. Zawadowski, J. von Delft, and D.C. Ralph, Phys. Rev. Lett. **83**, 2632 (1999).

[23] D.S. Golubev and A.D. Zaikin, Phys. Rev. Lett. **81**, 1074 (1998).

[24] A.B. Gougam, F. Pierre, H. Pothier, D. Esteve, and N.O. Birge, J. Low Temp. Phys. **118**, 447 (2000).

[25] F. Pierre and N.O. Birge, Phys. Rev. Lett. **89**, 206804 (2002); F. Pierre and N.O. Birge, J. Phys. Soc. Jpn. Suppl. A **72**, 19 (2003).

[26] J. Vranken, C. Van Haesendonck, and Y. Bruynseraede, Phys. Rev. B **37**, 8502 (1988).

[27] D.K. Wohlleben and B.R. Coles, *Magnetism*, edited by H. Suhl (Academic, New York, 1973), Vol. 5.

[28] The energy of the ions, 70 keV, was chosen to obtain an homogeneous concentration of manganese atoms in the thickness of the wires.

[29] V.I. Fal'ko, JETP Lett. **53**, 340 (1991).

[30] M.B. Maple, *Magnetism*, edited by H. Suhl (Academic, New York, 1973), Vol. 5.

[31] C. Van Haesendonck, J. Vranken, and Y. Bruynseraede, Phys. Rev. Lett. **58**, 1968 (1987).

[32] In vacuum, the magnetic moment of manganese atoms is $S=5/2$, but $S=5/2$ does not allow accurate fits of the measurements. It has been suggested that the random crystal field effectively reduces the degeneracy of the lowest-lying spin multiplet to a doublet, regardless of the actual spin of the magnetic impurity [L. Glazman (private communication)]. See also O. Ujsaghy, A. Zawadowski, and B.L. Gyorffy, Phys. Rev. Lett. **76**, 2378 (1996).

[33] A.C. Hewson, *The Kondo Problem to Heavy Fermions* (Cambridge University Press, Cambridge, 1993).

[34] The value of $B_K$ for low concentrations of iron in gold can be found for instance in P. Mohanty and R.A. Webb, Phys. Rev. Lett. **84**, 4481 (2000). This parameter is expected to be similar for other Kondo impurities in silver and copper.

[35] D.S. Golubev, A.D. Zaikin, and G. Schön, J. Low Temp. Phys. **126**, 1355 (2002).

[36] See J. von Delft, cond-mat/0210644, and references therein.

[37] D. Natelson, R.L. Willett, K.W. West, and L.N. Pfeiffer, Phys. Rev. Lett. **86**, 1821 (2001). In their article, the quantity Natelson *et al.* refer to as $\tau_\phi$ or $\tau_N$ is four times smaller than the phase

coherence time extracted from Eq. (1) [see Eq. (1) in Natelson *et al.*]. We took this correction into account in Fig. 8. Note that the diffusion coefficients used by Natelson *et al.* were obtained from the conductivity of co-evaporated thin films. Using the expected geometry and the measured resistance of the wires, as was done for all other samples, would give diffusion coefficients about twice smaller, which would move the open circles in Fig. 8 about one decade to the right, and slightly upward.

[38] D.S. Golubev and A.D. Zaikin, Phys. Rev. B **59**, 9195 (1999).

[39] A. Anthore, F. Pierre, H. Pothier, and D. Esteve, Phys. Rev. Lett. **90**, 076806 (2003); A. Anthore, F. Pierre, H. Pothier, D. Esteve, and M.H. Devoret, in *Electronic Correlations*: *From Meso- to Nano-Physics*, edited by T. Martin, G. Montambaux, and J. Trân Thanh Vân (EDP Sciences, New York, 2001); cond-mat/0109297.

[40] I.L. Aleiner, B.L. Altshuler, and Y.M. Galperin, Phys. Rev. B **63**, 201401 (2001).

[41] I.L. Aleiner, B.L. Altshuler, Y.M. Galperin, and T.A. Shutenko, Phys. Rev. Lett. **86**, 2629 (2001); I.L. Aleiner and D. Controzzi, Phys. Rev. B **66**, 045107 (2002).

[42] A. Zawadowski and G. Zarand, cond-mat/0009283; O. Ujsaghy, K. Vladar, G. Zarand, and A. Zawadowski, J. Low Temp. Phys. **126**, 1221 (2002).

[43] J.S. Meyer, V.I. Fal'ko, and B.L. Altshuler, *Strongly-Correlated Fermions and Bosons in Low-Dimensional Disordered Systems*, edited by I. Lerner, B.L. Altshuler, V.I. Fal'ko, and T. Giamarchi (Kluwer Academic, Dordrecht, 2002); cond-mat/0206024.

[44] A.G. Aronov and Y.V. Sharvin, Rev. Mod. Phys. **59**, 755 (1987); V. Chandrasekhar, Ph.D. thesis, Yale University, 1989. We neglect here the triplet contribution to AB oscillations since the spin–orbit length is much smaller than $L_\phi$.

[45] At 40 mK and low magnetic field, our experimental noise floor dominates the amplitude of conductance fluctuations in the $h/e$ frequency window. This explains the smaller relative increase of $\Delta G_{AB}$ at 40 mK compared to 100 mK.

[46] In principle, the constant $C$ in Eq. (13) is calculable from the known sample geometry. In practice, the calculation is quite difficult in four-terminal measurement geometry [Thomas Ludwig (private communication)]. See, D.P. DiVincenzo and C.L. Kane, Phys. Rev. B **38**, 3006 (1988); C.L. Kane, P.A. Lee, and D.P. DiVincenzo, *ibid.* **38**, 2995 (1988).

[47] M.G. Vavilov and L.I. Glazman, Phys. Rev. B **67**, 115310 (2003).

[48] Although the magnetic field dependence of the Vavilov-Glazman prediction depends on the spin $S$ of the magnetic impurity, the quality of the fit adjusting the parameter $g$ hardly changes with $S$, indicating that the noise in the data is too large to permit a reliable determination of $S$ in our samples.

[49] B.X. Yang, J.M. Tranquada, and G. Shirane, Phys. Rev. B **38**, 174 (1988).

[50] F. Pierre, H. Pothier, D. Esteve, M.H. Devoret, A. Gougam, and N.O. Birge, in *Kondo Effect and Dephasing in Low-Dimensional Metallic Systems*, edited by V. Chandrasekhar, C. Van Haesendonck, and A. Zawadowski (Kluwer, Dordrecht, 2001), p. 119; cond-mat/0012038.

[51] F. Pierre, H. Pothier, D. Esteve, and M.H. Devoret, J. Low Temp. Phys. **118**, 437 (2000).

[52] A. Kaminski and L.I. Glazman, Phys. Rev. Lett. **86**, 2400 (2001).

[53] It is not clear that the saturation of $\tau_\phi$ observed in strongly disordered alloys, cf. J.J. Lin, Y.L. Zhong, and T.J. Li, Europhys. Lett. **57**, 872 (2002), can be explained along the same lines.

[54] M. Henny, H. Birk, R. Huber, C. Strunk, A. Bachtold, M. Krüger, and C. Schönenberger, Appl. Phys. Lett. **71**, 773 (1997).

[55] F.C. Wellstood, C. Urbina, and J. Clarke, Phys. Rev. B **49**, 5942 (1992).

[56] Three parameters describing effects of electron–phonon scattering are used in this review: $B$ in Eq. (4), $\Sigma$ and $\kappa_{\rm ph}$ in Appendix A. They are related by the relations (Ref. 11), $\Sigma = 24\zeta(5)\nu_F\kappa_{\rm ph}k_B^5$ and $B = 6\zeta(3)\kappa_{\rm ph}k_B^3$, with $\zeta(x)$ the Riemann zeta function: $\zeta(5) \simeq 1.04$ and $\zeta(3) \simeq 1.2$. Introducing the heat capacity coefficient $\gamma$, one has the relation $\Sigma \simeq 1.05\gamma B$.

[57] A. Kamenev and A. Andreev, Phys. Rev. B **60**, 2218 (1999).

[58] We replaced the cut-off at $\hbar/\tau_\phi(T)$ by $\hbar/\tau_{ee}(T)$ whereas, when another inelastic process such as electron–phonon scattering limits the quantum coherence, the integral should be cut-off at $\hbar/\tau_\phi$ $(>\hbar/\tau_{ee})$. We neglect this correction here since it applies only when the contribution of electron–electron interactions is already weak.

[59] A.D. Benoit, S. Washburn, R.A. Webb, D. Mailly, and L. Dumoulin, *Anderson Localization*, edited by T. Ando and H. Fukuyama (Springer, Berlin, 1988).

[60] V.I. Fal'ko, J. Phys.: Condens. Matter **4**, 3943 (1992).